Available online at www.sciencedirect.com
SCIENCE DIRECT®
Polymer 45 (2004) 973–981
polymer
www.elsevier.com/locate/polymer

# Miscible blends of syndiotactic polystyrene and atactic polystyrene. Part 2. Depolarized light scattering studies and crystal growth rates

Chi Wang*, Wei-Po Liao, Ming-Ling Wang, Chang-Chun Lin

*Department of Chemical Engineering, National Cheng Kung University, 1, University Road, Tainan 701, Taiwan, ROC*

Received 9 August 2003; received in revised form 20 November 2003; accepted 4 December 2003

**Abstract**

Crystallization kinetics and morphology in miscible blends of syndiotactic polystyrene (sPS) and atactic postyrene (aPS) have been investigated by means of time-resolved depolarized light scattering (DPLS), polarized optical microscopy (POM) and scanning electron microscopy (SEM). Two different weight-average molecular weight of aPS, i.e. $M_w$ = 100k and 4.3k, were used to prepare the blends and denoted sPS/aPS(H) and sPS/aPS(M), respectively. Owing to a dilution effect, addition of aPS reduces the crystal growth rate and the overall crystallization rate of sPS; the reduction is more significant in sPS/aPS(M) of which a depression of equilibrium melting temperature is found due to the enhanced mixing entropy. Linear crystal growth is always observed in sPS/aPS(H) at the temperatures studied (240–269 °C) and results in an interfibrillar segregation morphology revealed by SEM, whereas sPS/aPS(M) with high aPS content exhibits non-linear growth behavior at low supercooling and gives an interspherulitic segregation morphology. Based on the Lauritzen–Hoffman theory, the fold surface free energies ($\sigma_e$) of sPS lamellae derived from DPLS and POM are in fair agreement, being 15.1 erg/cm$^2$ from the former and 12.6 erg/cm$^2$ from the latter. The peculiarly low values of $\sigma_e$ and the derived work of chain folding are discussed briefly. On addition of aPS, the lateral surface free energy of lamellae remains intact (9.9 erg/cm$^2$) regardless of aPS molecular weight used, which is ascribed to the absence of specific interaction between sPS and aPS components. Moreover, it seems that the activation energy for sPS chains to diffuse from the miscible melt to the crystal growth front is slightly increased in sPS/aPS(M), plausibly attributable to the extra energy required for the demixing process.


*Keywords:* Syndiotactic polystyrene; Blends; Growth rate

## 1. Introduction

Syndiotactic polystyrene (sPS) is a relatively new high performance polymer possessing high melting temperature and good chemical and solvent resistance, compared with its isomeric counterparts, isotactic PS (iPS) and atactic PS (aPS). In the past decade, many studies have been carried out to characterize the crystal structure [1–5], the miscibility with other polymers [6–8], and the crystallization of sPS and its blends with other polymers such as aPS, etc. [9–11]. Using differential scanning calorimetry (DSC), Wu and Woo [11] have conducted the Avarmi plots of sPS/aPS and sPS/PPO blends at various isothermal temperatures. Similar experiments on the neat sPS and sPS/aPS blends have been performed by Lawarence et al. [12] and Chiu et al. [13] using isothermal, and by Wesson [14] and Park et al. [15] using non-isothermal conditions. In general, the overall crystallization rate derived from the Avrami plot depends on the nucleation type as well as the crystal growth rate. Spherulitic growth rates of neat sPS and sPS/aPS blends have been measured using polarized optical microscopy (POM)[16–18]. However, to our best knowledge, there has been no crystallization studies so far reported on the light scattering of sPS/aPS blends. Moreover, in spite of the fact that the crystallization behavior of sPS and its blends have been investigated by various groups previously, the growth rate kinetics associated with the Lauritzen–Hoffman (LH) theory [19] involving the secondary nucleation process have seldom been reported [20,21]. In this paper, we examine the crystallization kinetics of sPS/aPS blends using POM as well as depolarized light scattering (DPLS) technique. Attempts are made at determining the surface free energies of lamellar crystals on the basis of LH theory. In addition, effect of aPS molecular weight (MW) on the crystallization of sPS will be

* Corresponding author. Tel.: +886-62378422; fax: +886-62344496.
*E-mail address:* chiwang@mail.ncku.edu.tw (C. Wang).

0032-3861/$ - see front matter © 2003 Elsevier Ltd. All rights reserved.
doi:10.1016/j.polymer.2003.12.008

discussed. In the athermal blends of sPS/aPS pair, it is expected that the application of low MW of aPS will enhance the entropy of mixing and leads to the variation of the crystallization window, defined by the glass transition and equilibrium melting temperatures of the blends.

## 2. Experimental

sPS pellets with a weight-average molecular weight, $M_w$, ~200k was supplied by Dow Chemical Co. Two aPS with different molecular weights ($M_w$ ~ 100k and 4.3k, referred to as aPS(H) and aPS(M), respectively) were purchased from Aldrich Co. To prepare sPS/aPS(H) blend, appropriate amounts of aPS and sPS were first dissolved in *ortho*-dichlorobenze (*o*-DCB) at 140 °C for 2 h with a polymer concentration of 1 wt%. The homogeneous solution was then poured into 20 fold excess volume of methanol for precipitation of sPS/aPS(H) blend powders. The blend powders were collected through filtration and vacuum dried to remove the residual solvents. To avoid the dissolution of low MW species of aPS(M) in the methanol in preparation of sPS/aPS(M) blends, the homogeneous solution was cast on glass dishes. Evaporation of *o*-DCB was allowed at ambient temperature for several days and further drying was carried out in a vacuum oven.

The DPLS measurements were conducted under a Hv polarization mode with a vertical setup for DPLS apparatus consisting of a 4 mW polarized He/Ne laser, analyzer, and a highly sensible CCD camera (Apogee, AP1) as the detector. Thin specimens, ca. 20 μm, was placed in a hot stage (Linkam, THMS600) in which thermal environment for crystallization was under programming control. For melt crystallization, the as-prepared specimens were first held at 300 °C for 10 min, and then cooled with a rate of 100 °C/min to the desired crystallization temperature $T_c$ for isothermal crystallization. Scattering images were recorded at a suitable time interval to reveal the details of crystallization evolution.

To observe the genuine morphology and the spherulitic growth, a polarized optical microscope (POM, Leica DMLP) was used as well. Radii of growing spherulites were measured continuously through a recording system until the impingement of spherulites. From the plot of spherulitic radius versus elapsed time, the linear slope denotes the crystal growth rate. The crystal modification of the crystallized samples was orthorhombic β′ form ($a = 0.881$, $b = 2.882$, and $c = 0.508$ nm [2,22]) as characterized by wide-angle X-ray diffraction. Morphology of lamellar stacks of sPS/aPS blends was investigated using scanning electron microscopy (SEM, Hitachi S4100). Prior to SEM observation, the isothermally crystallized thin films were etched using amyl acetate to wash away the aPS component. The etching procedure followed the method conducted by Kit and Schultz [23].

## 3. Results and discussion

### 3.1. DPLS studies on the melt crystallization of neat sPS

For all $T_c$ investigated, the four-leaf-clover imaging pattern which was typical for spherulitic entities was not observed when DPLS was conducted on neat sPS. Typical scattering intensity profiles during crystallization evolution are shown in Fig. 1, from which a monotonic decrease of scattered intensities with increasing scattering vector $q$ ($= 4\pi \sin\theta/\lambda$, where $\lambda$ is the wavelength of the laser light and $2\theta$ is the scattering angle) is found. The absence of the scattering maximum is evident for all crystallization time ($t_c$). Previously, we have already demonstrated that sPS spherulites as well as axilites are frequently found under POM observation, and the fraction of axilite content is rather high [16]. Thus, the DPLS patterns obtained from melt-crystallized samples are more likely to be representative of both spherulitic and rod-like morphologies. DPLS from the rod-like axilites will give a monotonic decay of intensity profile [24]. Our previous work demonstrated that spherulitic features are predominant at low $T_c$, whereas axilitic morphology is preferred at high $T_c$. However, the fraction of axilites is more than 0.4 regardless of $T_c$ investigated. It is concluded that the absence of scattering maximum is mainly attributed to the presence of large amounts of the axilitic superstructure, which significantly diminish the scattering peak induced by the spherulites. Although measurements of spherulitic (or axlitic) dimensions seem infeasible to further deduce the crystal growth rate, the scattering invariant approach provides an alternative route to describe the crystallization kinetics. The scattering invariant $Q$ can be determined by integrating the scattered Hv intensities over the entire $q$ and is given by Ref. [25]

$$Q = \int_0^\infty I_{Hv} q^2 dq \sim \langle \delta^2 \rangle \sim \Phi_d \Phi_c (\alpha_1 - \alpha_2)^2 F^2 \quad (1)$$

where $\langle \delta^2 \rangle$ represents the mean-square orientation

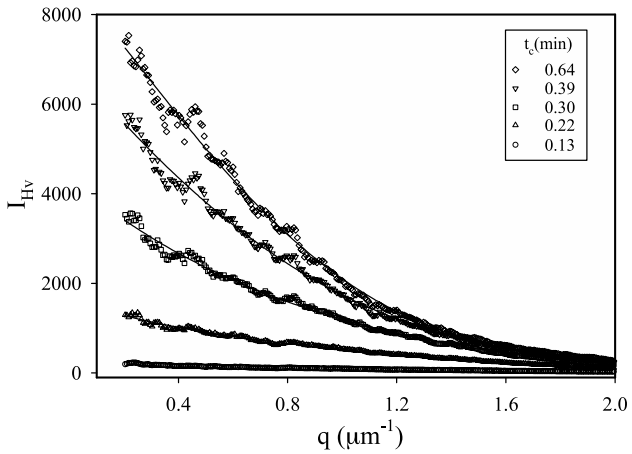


Fig. 1. Change in Hv light-scattering profile of neat sPS with time after the temperature drop from 300 to 240 °C (melt crystallization).

fluctuations and $\Phi_d$ is the volume fraction of the growing entities (spherulites or axilites), $\Phi_c$ is the volume fraction crystallinity within the entities, $F$ is a function to describe the crystal orientation within spherulites, and $\alpha_1$ and $\alpha_2$ are the parallel and perpendicular component of the polarizability. The variations of $\Phi_c$, $F$ and $\alpha_1 - \alpha_2$ are assumed to be negligible during crystallization, leading to that the Hv invariant should increase linearly with $\Phi_d$. Thus, time-resolved Hv scattering invariant approach is capable of detecting the crystallization kinetics together with the Avrami equation as follows [26,27],

$$\ln[-\ln(1 - Q_{norm})] = \ln k + n \ln t_c \quad (2)$$

where $k$ is the overall crystallization rate, $n$ is the Avrami exponent, and $Q_{norm}$ is the normalized Hv scattering invariant, which is given by the ratio of $Q(t_c)$ to $Q(t = \infty)$. Fig. 2 shows the derived $Q_{norm}$ versus crystallization time plots for neat sPS melt-crystallized at various $T_c$. As expected, a longer induction time ($t_i$) is required for crystallization to initiate at higher $T_c$. According to Eq. (2), typical Avrami plots are shown in Fig. 3 where $n$ and $k$ were obtained from the slope and intercept, respectively. As expected, the overall crystallization rate is reduced at high $T_c$. The derived exponent $n$ is ca. 3.0 for the $T_c$ range studied, implying heterogeneous nucleation and three-dimensional crystal growth, which is confirmed under POM observation. A simple relation between the crystal growth rate ($G$) and the Avrami parameters is given by: $G \sim k^{1/n}$. For crystallization at $T_c$ above $T_g + 100$ °C, the Arrhenius activation energy for diffusion is more representative than the WLF temperature dependence [19]. Thus, the crystal growth rates of a homopolymer are commonly described by the LH equation [19]

$$G = G_o \exp\left(-\frac{\Delta E}{RT_c}\right)\exp\left(-\frac{K_g}{fT_c\Delta T}\right) \quad (3)$$

where $\Delta E$ is the Arrhenius activation energy for segmental transportation, $\Delta T$ is the supercooling ($= T_m^o - T_c$, $T_m^o$ is the equilibrium melting temperature), $f$ is a corrected factor to account for the variation of heat of fusion at high supercoolings [$= 2T_c/(T_m^o + T_c)$], and $K_g$ is the nucleation constant, which is defined as $K_g = nb_o\sigma\sigma_e T_m^o/k\Delta H_f^o$, where $\Delta H_f^o$ is the heat of fusion, $b_o$ is the layer thickness, $\sigma$ is the lateral surface energy, and $\sigma_e$ is the fold surface energy. Depending on the growth regime, $n$ is 4 for regimes I and III and equals to 2 for regime II. Fig. 4 shows the values of $G$ estimated from the Avrami parameters as a function of $1/(fT_c\Delta T)$ using $\Delta E = 90$ kJ/mol [28] and $T_m^o = 291$ °C [29]. A straight line is obtained, suggesting that no regime transition in the $T_c$ range (240–265 °C) investigated. The best fit of a linear relationship to the data in Fig. 4 yields $K_g = 1.997 \times 10^5$ K$^2$ and $\log G_o = 12.910$. To deduce the morphological parameters from $K_g$, the growth regime can be assigned using the Z-test [30]. The growth plane is more likely to be (020) rather than (040) in consideration of the stacking fault behavior which is dominantly observed in the β′-form sPS [31,32]. To account for the stacking faults in the crystallites, Tosaka et al. [31] proposed that arrangement of neighboring two sPS chains in a special order has been developed in the vicinity of the growth front prior to being deposited on the crystal substrate. After being physically

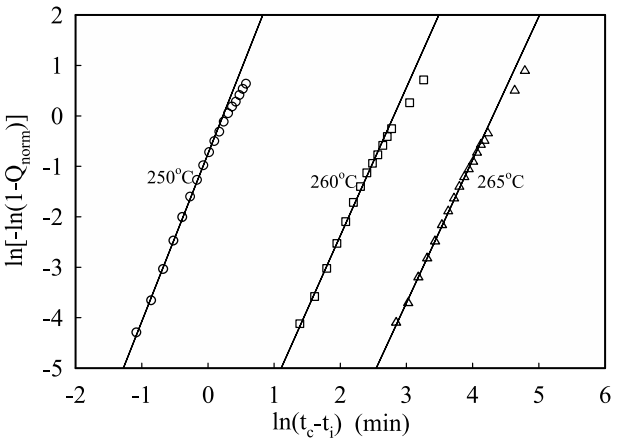


Fig. 3. Avrami plots of neat sPS at various temperatures.

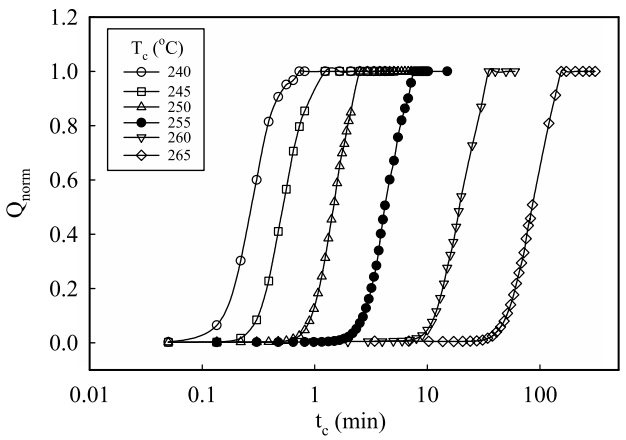


Fig. 2. Time variation of light-scattering invariant $Q$ for neat sPS during crystallization at various temperatures.

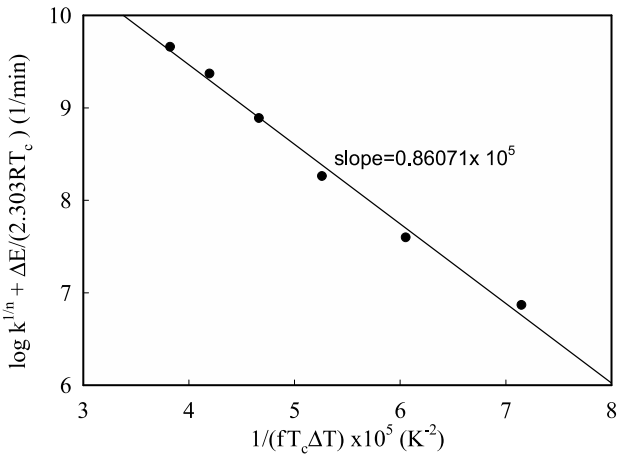


Fig. 4. Temperature dependence of linear crystallization rate obtained from DPLS.

adsorbed, these two sPS chains register into the crystal lattice in pair to develop a layer thickness ($b_o$) of 1.442 nm in forming a critical lamella. When the backbone chains fold due to a kinetic effect, ⟨100⟩ direction is assumed, giving a stem width ($a_o$) of 0.881 nm. It should be noted that two folds are developed in a crystal stem with a cross-section area of $a_o b_o$ when the bilayer-constituent chains re-enter the crystal. Using the Z-test and assuming regime *I* growth kinetics, we find the substrate length *L* smaller than 0.4 nm at $T_c = 250$ °C which is unlikely to occur in nature. On the other hand, the derived *L* is larger than 314 nm at $T_c = 250$ °C if regime II growth is assumed, which is reasonably acceptable in comparison with the lamellar thickness, ca. 6.3 nm determined from small-angle X-ray scattering in the preceding paper [33]. On the basis of regime II kinetics, the deduced $\sigma\sigma_e/\Delta H_f^o$ is ca. $1.696 \times 10^{-7}$ erg/cm. Using the Thomas–Staveley approximation [34] together with (020) plane growth, the derived value of $\sigma/\Delta H_f^o$ is ca. $1.127 \times 10^{-8}$ cm. Division of these two quantities each other leads to $\sigma_e = 15.0 \pm 0.6$ erg/cm$^2$. Previously, a similar value of $\sigma_e/\Delta H_f^o$ has been reported to be 0.2 nm obtained from single lamellar crystal measurements [32], and 0.12 nm derived from the Gibbs–Thomson equation [35]. When a $\Delta H_f^o$ value of 87.9 J/cm$^3$ [36] is substituted, the calculated $\sigma_e$ are ca. 17.6 and 10.5 erg/cm$^2$, respectively, which are in fair agreement with the present study by DPLS (15.0 ± 0.6 erg/cm$^2$).

In deriving $\sigma_e$ based on the LH theory, it has to be noted that a correctly chosen $T_m^o$ is escessentially important; whereas the influence of $\Delta E$ is relatively neglegible. Different $T_m^o$ selected for analysis will lead to the difference in the growth regime, which in turn gives inconsistent values of $\sigma_e$. There are conflicting $T_m^o$ values reported by several groups and a detailed discussion has been provided recently [35], suggesting that a reasonably consistent $T_m^o$ should fall in a range of 291–292.7 °C estimated from both the Gibbs–Thomson plot and the linear Hoffman–Weeks plot. Table 1 lists the $T_m^o$-dependence of regime-growth parameters deduced from LH theory. It is evident that a too high $T_m^o$ will lead the growth regime from II to I, which seems unrealistic in consideration of the high supercooling ($\Delta T \sim 40$K) produced. Previously we have also used an over-estimated $T_m^o$ value (312 °C) [37,38], obtained from the $T_c$-dependence of growth rate proposed by Marand et al. [39,40], to derive the $\sigma_e$ of 40.8 ± 0.2 erg/cm$^2$ [37], which is apparently too large, too. Although the present $T_c$ studied covers 25 °C range (240–265 °C), it seems that huge collection of growth rate data is a critical prerequisite if one intends to follow the Marand's approach to deduce both $T_m^o$ and $\sigma_e$ precisely [40].

Table 1
$T_m^o$ dependence of thermodynamic parameters of neat sPS derived from Hoffman–Lauritzen theory (DPLS results)

| Assumed $T_m^o$ (°C) | $K_g$ (K$^2$) | Regime[a] | $\sigma\sigma_e$ (erg$^2$/cm$^4$) | $\sigma_e$ (erg/cm$^2$) |
|---|---|---|---|---|
| 291[b] | $1.997 \times 10^5$ | II | 149.1 | 15.1 |
| 292.7[c] | $2.185 \times 10^5$ | II | 162.6 | 16.4 |
| 320[d] | $6.948 \times 10^5$ | I | 246.7 | 24.9 |

[a] Judging from the Z-test [30].
[b] Ref. [29], based on the linear Hoffman–Weeks plot
[c] Ref. [35], based on the Gibbs–Thomson plot.
[d] Ref. [29], based on the non-linear Hoffman–Weeks plot.

### 3.2. DPLS studies on the melt crystallization of sPS/aPS blends

Absence of four-leaf-clover pattern was also found when DPLS was conducted on sPS/aPS blends melt-crystallized at 250 °C. The evolution of scattering invariant with $t_c$ is depicted in Fig. 5 for sPS/aPS(H) blends. For sPS/aPS(M) blends, similar results are obtained. It is evident that longer induction time is required to initiate the crystallization for blends with higher aPS content. Based on Eq. (2), the Avarmi parameters (*n* and *k*) are derived. The exponent is ca. 3.4 for all the blends, and together with *k* value the crystal growth rate can be estimated, as mentioned previously. Addition of amorphous aPS will reduce the content of crystallizable sPS chains at the crystal growing fronts due to a dilution effect. To a first approximation, it might be predicted that the linear growth rate *G* in a sPS/aPS blend is proportional to the volume fraction of crystallizable sPS, $\phi_{sPS}$, i.e. $G \sim \phi_{sPS}$ [20,41]. Thus, a pre-factor $\phi_{sPS}$ is suggested to add in the right-hand side of Eq. (3) to describe the $T_c$ and composition dependences of *G* in sPS/aPS blends. However, Inoue et al. [26] suggested that the appropriate pre-factor should be $\phi_{sPS}^{1/2}$ for regime II growth rather than $\phi_{sPS}$, which holds valid merely for the crystal growth in regimes I and III. Their conclusion came from the hypothesis of the two-step diffusion mechanism, i.e. the diffusion coefficients in the surface nucleation process and the substrate completion process should be distinguished from each other. To verify the composition dependence of *G*, Fig. 6 shows the log *G* versus log $\phi_{sPS}$ for sPS/aPS blends all crystallized at 250 °C. It should be emphasized

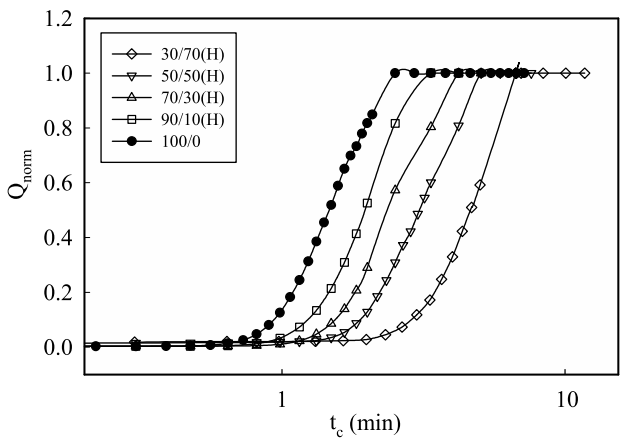


Fig. 5. Time variation of light-scattering invariant *Q* of sPS/aPS(H) blends during crystallization at 250 °C.

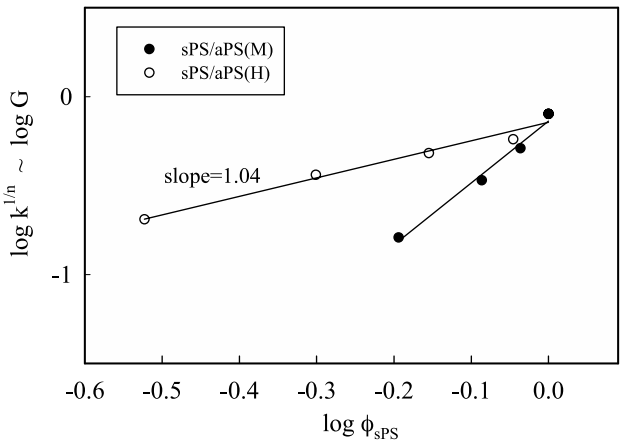


Fig. 6. Variation of crystallization rate with weight fraction of aPS in the sPS/aPS blends.

that the sPS/aPS(H) blends follow a linear line with a slope of unity. In other words, a pre-factor of $\phi_{sPS}$ used in Eq. (3) is more appropriate in the present blends although regime II growth prevails in these blends (as discussed later from POM results). From Fig. 6, apparently a steeper slope is obtained for sPS/aPS(M) blends. The discrepancy for sPS/aPS(M) is ascribed to the $T_m^o$ depression in the blend, resulting from the enhanced entropy of mixing when low molecular weight aPS is used. Analysis of the depression of $T_m^o$ via Flory–Huggins treatments [42], has been conducted and deduced $T_m^o$ values are tabulated in Table 2; $T_m^o$ is essentially reduced as aPS(M) concentration increases. At a given $T_c$ (250 °C), the depression of $T_m^o$ in sPS/aPS(M) blends will give a low supercooling, which in turn further reduces the crystal growth rate. On the other hand, $T_m^o$ of sPS/aPS(H) remains relatively unchanged regarless of the aPS(H) amount applied, leading to the simple relation

Table 2
Glass transition temperature ($T_g$), equilibrium melting temperature ($T_m^o$) and fold surface energy ($\sigma_e$) of sPS/aPS blends determined from POM measurements

| sPS/aPS | $T_g$ (°C)[a] | $T_m^o$ (°C)[b] | $\sigma\sigma_e$ (erg$^2$/cm$^4$) | $\sigma$ (erg/cm$^2$)[c] |
|---|---|---|---|---|
| 100/0 | 95.0 | 291.0 | 124.8 ± 1.0 | 9.9 |
| 70/30(H) | 97.6 | 290.9 | 124.8 ± 6.3 | 9.9 ± 0.5 |
| 50/50(H) | 98.3 | 290.8 | 118.5 ± 3.5 | 9.4 ± 0.3 |
| 30/70(H) | 98.9 | 290.7 | 129.7 ± 2.8 | 10.3 ± 0.2 |
| 92/8(M) | 94.5 | 290.4 | 119.2 ± 2.1 | 9.5 ± 0.2 |
| 82/18(M) | 91.8 | 289.6 | 124.1 ± 2.8 | 9.8 ± 0.2 |
| 64/36(M) | 89.2 | 288.3 | 126.9 ± 2.1 | 10.1 ± 0.2 |

[a] Determined from the DSC heating scan of amorphous samples at 10 °C/min.
[b] Estimated from the Flory–Huggins equation [42] with interaction parameter $\chi = 0$.
[c] $\sigma$ of neat sPS is calculated to be 9.9 erg/cm$^2$ using Thomas–Staveley approximation: $\sigma/\Delta H_f^o = \alpha(a_o b_o)^{1/2}$ where $\alpha \sim 0.1$ for vinyl polymers [45], and $a_o$ and $b_o$ are stem width and layer thickness, respectively. For (020) plane growth, $b_o = 1.44$ nm and $a_o = 0.881$ nm. Thus, the $\sigma_e$ of sPS lamella is 12.6 erg/cm$^2$. $\sigma$ of the blends are determined from $\sigma\sigma_e/\sigma_e$, assuming $\sigma_e$ is constant (12.6 erg/cm$^2$) in all the blends.

depicted in Fig. 6. Also given in Table 2 are the glass transion temperatures ($T_g$) of the glassy sPS/aPS blends determined from the differential scanning calriometry. The decrease of $T_g$ with increasing aPS(M) content implies the chain mobility is enhanced in sPS/aPS(M) in comparison with sPS/aPS(H) of which $T_g$ increases with increasing aPS(H) content.

### 3.3. POM observation of neat and sPS/aPS blends

Our previous report [16] has already shown that both positively birefringent spherulites and axlites observed at all $T_c$ under POM observation, but the amount of axilites increases at high $T_c$. Moreover, both spherulites and axiltes possess the same crystal growth rate at a given $T_c$. Fig. 7 shows the LH plot of POM results of neat sPS from which no growth transition is evident. Using the linear slope obtained from the regression analysis, $K_g$ is derived to be ca. $1.667 \times 10^5$ K$^2$, giving to $\sigma_e$ of 12.5 erg/cm$^2$, which is in fair agreement with that obtained from DPLS.

The variation of $G$ with $T_c$ is shown in Fig. 8(a) for sPS/aPS(H) blends and in Fig. 8(b) for sPS/aPS(M) blends. The measured $G$ is reduced by either increasing $T_c$ or by the addition of aPS component. Compared with neat sPS, the retardation of $G$ is more significant in sPS/aPS(M) than that in sPS/aPS(H) at a given $T_c$. As mentioned previously, the observed reduction of $G$ of sPS in its blends with aPS is a combined result of dilution effect and of $T_m^o$ depression, if any. Fig. 9 shows the modified LH plots for the sPS/aPS blends with both effects considered. A superposition of all sPS/aPS(H) data with various aPS contents is shown in Fig. 9(a), indicating that no change in the growth regime in the blend. Furthermore, the reduction of crystal growth is exclusively attributed to the dilution effect since no specific interaction between sPS and aPS exists. For sPS/aPS(M) blends, superposing the data for various aPS contents also gives a master curve but a small vertical drop is obvious

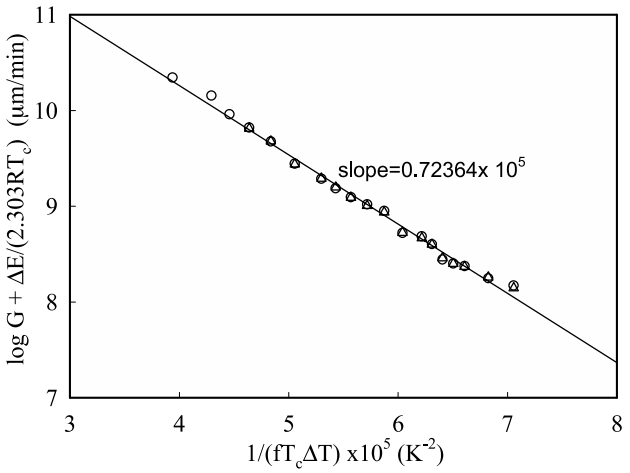


Fig. 7. Temperature dependence of crystal growth rate of neat sPS obtained from POM (open circles and triangles are growth rates for the spherulites and axilites, respectively. Data taken from Fig. 1 in Ref. [16]).

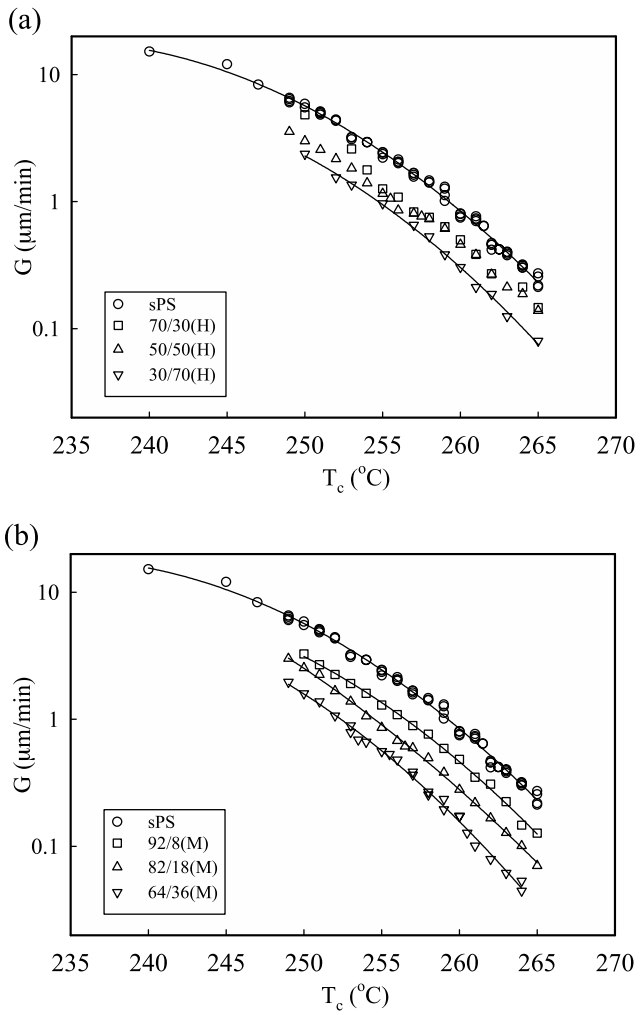


Fig. 8. Crystal growth rate $G$ of sPS/aPS blends at various crystallization temperatures, (a) sPS/aPS(H) blends, and (b) sPS/aPS(M) blends.

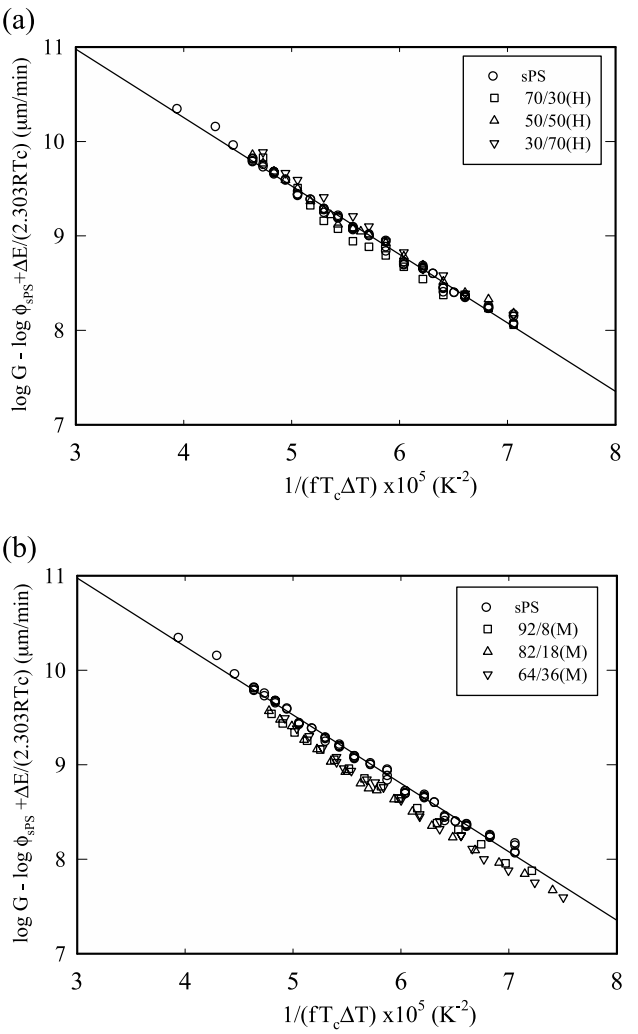


Fig. 9. Temperature dependence of crystal growth rate of sPS/aPS blends, (a) sPS/aPS(H) blends, and (b) sPS/aPS(M) blends. The solid line is the linear regression plot of neat sPS data.

from the data for neat sPS. To compensate this gap, it is found that a slightly higher activation energy (ca. 95 kJ/mol) is required for the chain diffusivity of sPS/aPS(M) in constructing the LH plot to superpose on the neat sPS data. It should be noted that the entropy of mixing is pronounced in sPS/aPS(M) due to the low MW of aPS. Thus, this extra energy seems relevant to the additional energy barrier for sPS demixing from the melt prior to its diffusion to the crystal growth front.

The values of $\sigma\sigma_e$ are calculated from $K_g$ obtained from the slopes in Fig. 9 and are given in Table 2. From the morphology investigation (discussed in Section 3.4), it has been found that aPS(H) and aPS(M) diluents are expelled out of the interlamellar regions, to reside in interfibrillar regions and/or interspherulitic regions depending on the crystallization conditions. Since the melt-fold interfacial region between lamellar crystals is not altered upon aPS blending, the value of $\sigma_e$ is assumed to be independent of the blend composition. On this basis, the lateral interfacial free energy, $\sigma$, is further deduced and tabulated in Table 2 as well. It is of interest to note that a constant $\sigma$ is obtained, which is in good agreement with the prediction by Huang and Marand [43] who have pointed out that $\sigma$ is independent of blend composition for athermal polymer blends.

### 3.4. Segregation of aPS in sPS/aPS blends

Although sPS/aPS forms a miscible blend in the melt, phase separation occurs during crystallization of the sPS component. The non-crystallizable aPS chains are rejected from the sPS crystals, resulting in three distinct modes of rejection: interlamellar, interfibrillar or interspherulitic, depending on the segregation length. As pointed out by Keith and Padden [44], the segregation length ($\delta$) is dependent on the relative ratio of aPS diffusivity ($D$) to the growth rate of sPS, i.e. $\delta = D/G$. Interfibrillar segregation is observed in all sPS/aPS(H) investigated here. Typical SEM images are shown in Fig. 10A and B for 50/50(H) crystallized at 252 and 269 °C, respectively. It should be noted that the aPS component was washed away

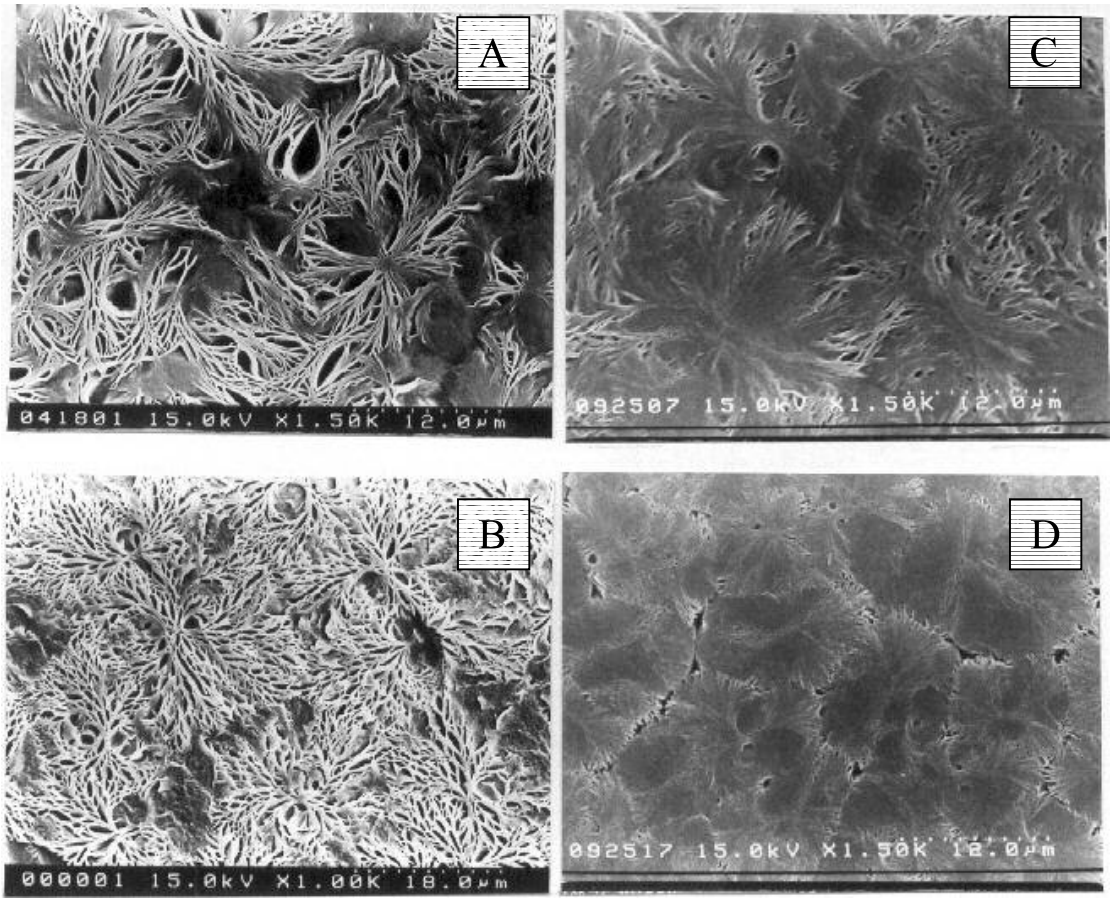


Fig. 10. SEM images of sPS/aPS blends revealing the placement of aPS after the crystallization of sPS. A: 50/50(H) $T_c = 252$ °C, B: 50/50(H) $T_c = 269$ °C, C: 82/18(M) $T_c = 252$ °C, and D: 82/18(M) $T_c = 269$ °C. Note the difference in the magnification.

using amyl acetate/ethanol solution, leaving sPS lamellar stacks for the detailed SEM observation. For sPS/aPS(H) blends, it is evident that placement of aPS is mainly between sPS lamellar stacks. This is consistent with the preceding paper which has investigated the lamellar morphology of sPS/aPS(H) using transmission electron microscopy [33]. The size distribution of the segregated aPS domains is more uniform for sPS/aPS(H) crystallized at higher $T_c$. At low $T_c$, fast nucleation and crystal growth lead to the interior of spherulites (or axilites) less ordered. For sPS/aPS(M) blends, interfibrillar aPS segregation also occurs at low $T_c$ (Fig. 10C), whereas a gradual transition to the interspherulitic segregation is observed at high $T_c$ as shown in Fig. 10D where the spherulitic boundary is readily observed. Indeed, the crystal growth rate is slower at longer $t_c$ and non-linear crystal growth is observed due to the deficiency of crystallizable sPS chains when interspherulitic segregation becomes dominant. The morphological transition for sPS/aPS(M) is not unexpected in consideration of the low $G$ at low supercooling, coupled with a large D of aPS(M) because of its low MW. To sum up, interlamellar aPS segregation is excluded in all the blends studied regardless of the aPS MW. It suggests that the environment of folded lamellar surface remains similar in the neat sPS and sPS/aPS blends, supporting the assumption of constant $\sigma_e$ used earlier to derive the $\sigma$ from the growth rate data.

### 3.5. Further comments on $\sigma_e$ of sPS

Using PE fragment decoration method as well as atomic force microscopy (AFM), Tosaka et al. [31] have investigated the characters of fold surface of sPS lamellar single crystals prepared from solution crystallization. Results showed that the vapor-deposited PE fragments are oriented randomly on the fold surface and there is no difference in AFM images between the parallel and perpendicular directions to the growth plane of sPS lamella, leading to the conclusion that sPS chains are folded in an irregular manner even in single crystals. For bulk crystallization as conducted in this study, the fold surface of sPS lamellae is expected to be more irregular due to the presence of entanglements which retrains the chain mobility. The loose loop developed for a chain fold suggests that some non-adjacent re-entry probably occurs in the growth plane in regime II where numerous nuclei form on the substrate simultaneously but spread slowly. The irregular chain folding may reasonably account for the unusually low value of $\sigma_e$ (12.6–15.1 erg/cm$^2$) for sPS lamellae, compared

to $\sigma$ (9.9 erg/cm$^2$). Normally, $\sigma_e$ is much larger (ca. 4–8 times) than $\sigma$ since work has to be done to fold the chain back into the lamellae. To estimate the work ($q$) required for chain folding, we tentatively assume adjacent re-entry and use the relation for calculation: $q = \sigma_e(a_o b_o)$, i.e. two folds are developed for a cross-sectional area of $a_o b_o$ due to the bimolecular-layer packing [32]. In spite of the presence of the bulky side ring, the deduced $q$ for sPS is only ca. 2.3–2.8 kcal/mol, which is much lower than that of PE (Table 3). Table 3 lists the tacticity effect of PS and polypropylene (PP) on the kinetics parameters derived from the crystal growth results, along with PE for a comparison purpose. It is of interest to note that syndiotactic isomer has lower values of $\sigma_e$ and $q$, compared with the isotactic isomer. In general, the amount of $q$ is related to two main factors; one is the number of bonds required to develop a fold and the other is the energy difference between the gauche and trans conformations. Wu [48] and Eckstein et al. [49] have shown that isotactic chains are less entangled in the molten state since they are more expanded than syndiotactic ones. In other words, the chain flexibility of sPS is better in comparison with iPS, suggesting that less bond numbers are involved in making a chain folding for sPS. In crystallites, the chain conformation is helix for iPS (iPP) but is planar zigzag for sPS (sPP). The significant low values of $q$ and $\sigma_e$ of sPS may be also due to the presence of predominantly all-trans conformations in the molten state [50] in contrast with iPS which is likely to form a random coil conformation [49]. As a consequence, smaller conformation distortions from the potential minima are expected for sPS chains, in contrast with iPS, in order to re-enter the crystal in the required crystallographic position. Recently, Napolitano et al. [51] used the molecular mechanics to simulate the adjacent re-entry folds of sPS chains. They calculated the q for an isolated sPS chain to be ranging from 12.0–20.3 kcal/mol, which is seemingly a quite high value with respect to the present measurements.

## 4. Conclusions

In miscible blends of sPS and aPS, both components have the same repeating unit, which leads to the absence of any specific interaction although the tacticity is different from each other. Without specific interaction between the two components, the crystallization of sPS/aPS blends is mainly dependent on two factors, i.e. the dilution effect due to the reduction of the crystallizable sPS chains at the crystal growth front, and the depression of $T_m^o$ caused commonly by the miscible blending. Thus, sPS/aPS blends provide a simple but exclusive model to investigate each effect on the crystallization kinetics of the blends if we carefully select the aPS component for the blend. High molecular weight aPS(H) is used in this study to maintain $T_m^o$, leaving the dilution effect to be discussed exclusively. On the other hand, addition of low molecular weight aPS(M) alters the dilute composition as well as $T_m^o$, giving rise to a more complex kinetics. By means of DPLS and POM, the crystal growth rates of the neat sPS were measured at various crystallization temperatures, and the derived fold surface free energies of sPS lamellae on the basis of the Lauritzen–Hoffman theory are in fair agreement. For sPS/aPS(H), the crystallization kinetics can be nicely interpreted by the modified LH theory involving the dilution effect only. For sPS/aPS(M), LH theory is also applicable if both dilution effect and $T_m^o$ depression are taken into consideration. On addition of aPS, the lateral surface free energy of sPS lamellae remains intact regardless of aPS molecular weight used, which is ascribed to the althermal character of this specific blend. Moreover, it seems that the activation energy for sPS chains to diffuse from the miscible melt to the crystal growth front is slightly increased in sPS/aPS(M), plausibly attributable to the extra energy required for the demixing process.

Table 3
Effect of tacticity on the kinetic results of PS and PP

| | $T_m^o$ (K) | $\sigma$ (erg/cm$^2$) | $\sigma_e$ (erg/cm$^2$) | $q$ (kcal/mol) | Ref. |
|---|---|---|---|---|---|
| PE | 418.5 | 11.8 | 90 | 4.9 | [45] |
| Syndiotactic-PP | 433 | 10.4–12.1 | 44.5 | 5.3 | [46] |
| Isotactic-PP | 458 | 11.1–11.9 | 67.5 | 6.6 | [47] |
| Isotactic-PS | 515 | 6.63 | 35 | 6.97 | [45] |
| Syndiotactic-PS | 564 | 9.9 | 12.6–15.1 | 2.3–2.8 | This work |

## Acknowledgements

This work has been supported through a grant from the National Science Council of the Republic of China (NSC91-2216-E-006-031).

## References

[1] Greis O, Xu Y, Asano T, Petermann J. Polymer 1989;30:590.
[2] Guerra G, Vitagliano VM, De Rosa C, Petraccone V, Corradini P. Macromolecules 1990;23:1539.
[3] Chatani Y, Shimane Y, Ijitsu T, Yukinari T. Polymer 1993;34:1625.
[4] De Rosa C. Macromolecules 1996;29:8460.
[5] Tosaka M, Hamada N, Tsuji M, Kohjiya S. Macromolecules 1997;30:6592.
[6] Guerra G, De Rosa C, Vitagliano VM, Petraccone V, Corradini P. J Polym Sci, Polym Phys Ed 1991;29:265.
[7] Hong BK, Jo WH, Kim J. Polymer 1998;39:3753.
[8] Bonnet M, Buhk M, Trögner G, Rogausch KD, Petermann J. Acta Polym 1998;49:174.
[9] Cimmino S, Di Pace E, Martuscelli E, Silvestre C. Polymer 1993;34:2799.
[10] Guerra G, De Rosa C, Vitagliano VM, Petraccone V, Corradini P, Karasz FE. Polym Commun 1991;32:30.
[11] Wu FS, Woo EM. Polym Engng Sci 1999;39:825.
[12] Lawarence SST, Shinozaki DM. Polym Engng Sci 1997;37:1825.
[13] Chiu FC, Peng CG. Polymer 2002;43:4879.

[14] Wesson RD. Polym Engng Sci 1994;34:1157.
[15] Park JY, Kwon MH, Park OO. J Polym Sci, Polym Phys Ed 2000;38: 3001.
[16] Wang C, Chen CC, Cheng YW, Liao WP, Wang ML. Polymer 2002; 43:5271.
[17] Cimmino S, Di Pace E, Martuscelli E, Silvestre C. Polym Commun 1991;32:251.
[18] Woo EM, Wu FS. J Polym Sci, Polym Phys Ed 1998;36:2725.
[19] Hoffman JD, Miller RL. Polymer 1997;38:3151.
[20] Duff S, Tsuyama S, Iwamoto T, Fujibayashi F, Birkinshaw C. Polymer 2001;42:991.
[21] Chen Q, Yu Y, Na T, Zhang H, Mo Z. J Appl Polym Sci 2002;83: 2528.
[22] Chatani Y, Fuji Y, Shimane Y, Ijitsu T. Polym Preprints Jpn (Eng Ed) 1988;37:E428.
[23] Kit KM, Schultz JM. J Polym Sci, Polym Phys Ed 1998;36:873.
[24] Hashimoto T, Ebisu S, Kawai H. J Polym Sci, Polym Phys Ed 1981; 19:59.
[25] Koberstein J, Russell TP, Stein RS. J Polym Sci, Polym Phys Ed 1979; 17:1719.
[26] Okamoto M, Inoue T. Polymer 1995;36:2739.
[27] Isayeva I, Kyu T, Manley RSJ. Polymer 1998;39:4599.
[28] Tirrell M. Rubber Chem Technol 1984;57:523.
[29] Wang C, Hsu YC, Lo CF. Polymer 2001;42:8447.
[30] Lauritzen JI, Hoffman JD. J Appl Phys 1973;44:4340.
[31] Tosaka MM, Hamada N, Tsuji M, Kohjiya S, Ogawa T, Isoda S, Kobayashi T. Macromolecules 1997;30:4132. For sPS crystallized from the melt, the fold surface of lamellae is expected to be rather irregular since irregular chain folding is observed even in the single crystals of sPS detected in this article.
[32] Tosaka M, Hamada N, Tsuji M, Kohjiya S. Macromolecules 1997;30: 6592.
[33] Wang C, Liao WP, Cheng YW, Lin TL. Jpol. In press.
[34] Thomas DG, Staveley LAK. J Chem Soc 1952;4569.
[35] Wang C, Cheng YW, Hsu YC, Lin TL. J Polym Sci, Polym Phys Ed 2002;40:1626. A precise value of $\sigma_e/\Delta H_f^o$ is ca. 0.12 nm calculated from the linear slope of Fig. 10, rather than the mis-given value reported in the article.
[36] Gianotti G, Valvassori A. Polymer 1990;31:473. A different value of $\Delta H_f^o$ is reported by Paszlor et al. to be ca. 53.2 J/g: Paszlor JR, Landes BG, Karjala PJ. Thermochim Acta 1991;177:187.
[37] Wang C, Chen CC. Polym Bull 1999;43:433.
[38] Chen CC. Master Thesis, Yuan-Ze University, Taiwan 1999.
[39] Xu J, Srinivas S, Marand H, Agarwal P. Macromolecules 1998;31: 8230.
[40] Huang J, Parasad A, Marand H. Polymer 1994;35:1896.
[41] Alfonso GC, Chiappa V, Liu J, Sadiku ER. Eur Polym J 1991;27:795.
[42] Flory PJ. Principles of polymer chemistry. Ithaca, NY: Cornell University Press; 1953. Nishi T, Wang TT. Macromolecules 1975;8: 909.
[43] Huang J, Marand H. Macromolecules 1997;30:1069.
[44] Keith HD, Padden FJ. J Appl Phys 1964;35:1270.
[45] Hoffman JD, Miller RL, Marand H, Roitman DB. Macromolecules 1992;25:2221.
[46] Arnold JR, Bu Z, Cheng SZD, Hsieh ET, Johnson TW, Geerts RG, Palackal SJ, Hawley GR, Welch MB. Polymer 1994;35:5197.
[47] Clark EJ, Hoffman JD. Macromolecules 1984;17:878.
[48] Wu S. J Polym Sci, Polym Phys Ed 1989;27:723.
[49] Eckstein A, Suhm J, Friedrich C, Maier RD, Sassmannshausen J, Bochmann M, Mülhaupt R. Macromolecules 1998;31:1335.
[50] Matsuba G, Kaji K, Nishida K, Kanaya T, Imai M. Macromolecules 1999;32:8932.
[51] Napolitano R, Pirozzi B. Macromol Theory Simul 2002;11:472.